Proceedings of the 29th International Conference on Ocean, Offshore and Arctic Engineering
OMAE2010
June 6 - 11 , 2010, Shanghai, China

OMAE2010-20991

ON THE VORTEX-INDUCED VIBRATION RESPONSE OF A MODEL RISER AND LOCATION OF SENSORS FOR FATIGUE DAMAGE PREDICTION

C. Shi
Dept. of Civil, Arch., and Env. Engineering
University of Texas
Austin, TX 78712, USA
Email: cshi@mail.utexas.edu

L. Manuel*
Dept. of Civil, Arch., and Env. Engineering
University of Texas
Austin, TX 78712, USA
Email: lmanuel@mail.utexas.edu

M. A. Tognarelli
BP America Production Co.
Houston, TX 77079, USA
Email: Michael.Tognarelli@bp.com

T. Botros
BP America Production Co.
Houston, TX 77079, USA
Email: Tammer.Botros@bp.com

ABSTRACT

This study is concerned with vortex-induced vibration (VIV) of deepwater marine risers. Riser response measurements from model tests on a densely instrumented long, flexible riser in uniform and sheared currents offer an almost ideal set-up for our work. Our objectives are two-fold: (i) we use the measured data to describe complexities inherent in riser motions accompanying VIV; and (ii) we discuss how such data sets (and even less spatially dense monitoring) can be used effectively in predicting fatigue damage rates which is of critical interest for deepwater risers.

First, we use mathematical tools including Hilbert and wavelet transforms to estimate instantaneous amplitudes and phases of cross-flow (CF) and in-line (IL) displacements for the model riser as well as scalograms to understand time-frequency characteristics of the response; this work confirms that the motion of a long flexible cylinder is far more complex than that of a rigid cylinder, and that non-stationary characteristics, higher harmonics, and traveling waves are evident in the riser response. Second, a well-established empirical procedure, which we refer to as Weighted Waveform Analysis (WWA), is employed to estimate the fatigue damage rate at various locations along the length of the riser from strain measurements at only eight sensors. By iterating over numerous different combinations of these eight strain sensors as inputs (from among all the twenty-four available locations on the riser), optimal locations for the eight sensors on the riser are identified by cross-validation, whereby predicted strains and fatigue damage rates at locations of instrumented sensors are compared with strains and fatigue damage rates based on actual recorded measurements there. We find that, if properly placed, as few as eight sensors can provide reasonably accurate estimates of the fatigue damage rate over the entire riser length.

Finally, we demonstrate how more accurate fatigue damage prediction can result when non-stationary response characteristics are considered and a modified WWA method (that more effectively accounts for traveling waves than the WWA method alone does) is employed.

INTRODUCTION

Vortex-Induced Vibration (VIV) is of great interest in the context of fatigue design of marine risers as oil and gas production moves into deeper waters. Model tests provide valuable insight into the VIV phenomenon and associated riser response characteristics. Experiments, especially on long flexible cylinders, which better resemble real deepwater marine risers, help to study more complex response features than those conducted on short rigid cylinders under similar current/flow conditions [1].

In this study, measurements (strains and accelerations) available from the Norwegian Deepwater Programme (NDP) experiments on an instrumented riser are employed to examine the characteristics of the VIV response of a long flexible cylinder (model riser) placed in uniform or sheared currents.

*Corresponding Author

Instantaneous amplitudes of the CF and the IL displacements, as well as the phase difference between the CF and IL displacements (based on the phase angles associated with the motion orbits), are estimated from their analytic signals obtained using Hilbert transforms. The varying spatial patterns of displacement amplitudes and phase angles (motion orbits) over the riser length confirm that the motion of a long flexible cylinder is far more complex than that of a rigid cylinder; similarly, the temporal variation in riser response, even within a single recorded event where the current velocity profile is unchanged, illustrates non-stationary behavior which is more pronounced for uniform current profiles than for sheared currents.

Wavelet transforms offer useful time-frequency representations of complex response such as that from VIV of risers. Using continuous wavelet transforms, the energy content in a signal in the time and frequency domains can be represented using scalograms which, on one plot, describe time, scale (related to frequency), and wavelet transform coefficient value (where the latter is often squared and shown by varying intensity or color). In this study, scalograms of the measured NDP model riser strains reveal that (i) higher harmonics are commonly observed when the riser is subjected either to uniform or sheared currents; and (ii) the energy distribution among the first and higher harmonics can vary considerably even within one record, especially for uniform current profiles.

Besides non-stationary characteristics and the presence of higher harmonics in the response, the occurrence of traveling waves along the NDP model riser, when subjected either to uniform or sheared currents, is observed in the data. Such traveling wave influences are noted while studying the riser response.

Beyond studies of the riser motions and strains, our interest is in estimation of fatigue damage rates over the entire length of the riser using an empirical procedure—Weighted Waveform Analysis (WWA)—while making use of the NDP data. Application of the WWA procedure to riser response reconstruction and to fatigue damage estimation may also be found in other studies [2] and [3]. There are, however, some differences in the application of the WWA procedure as it is carried out here versus that in the cited publications. First, instead of filtering out the higher harmonics in the strain time series, in the present study, important frequency components including the first as well as higher harmonics, are all preserved and reconstructed as part of the empirical procedure. Second, the earlier studies used measurements from a large number of sensors to fit to the WWA model. For example, when analyzing the CF response of the NDP model riser, Trim, et al. [2] used measurements from all the thirty-two sensors (twenty-four strain sensors and eight accelerometers). Due to the excessive cost of full-scale field studies, drilling risers in such full-scale measurement campaigns are rarely as densely instrumented as the NDP model riser; our interest is in accurate estimation of the fatigue damage rate over the entire length of the riser using only a small number of sensors. Accordingly, in this study, the WWA procedure is applied using measurements from only eight strain sensors. By iterating over numerous different combinations of the selected eight strain sensors as inputs (from among all available choices), optimal locations for the eight sensors on the riser are identified by cross-validation, whereby predicted strains and fatigue damage rates at locations of instrumented sensors are compared with strains and fatigue damage rates based on actual recorded measurements there. We shall show that, if properly placed, as few as eight sensors can provide reasonably accurate estimates of the fatigue damage rate over the entire riser length. We also show very briefly, with an example, that by correcting for non-stationary response characteristics and by employing a modification to the WWA method that more directly accounts for traveling wave characteristics, improved accuracy in fatigue damage prediction is possible.

Table 1. The four bare riser NDP data sets.

Event no.	Current profile	Max. current speed (m/s)	Largest RMS CF-disp/D
2120	Uniform	1.4	0.44
2150	Uniform	1.7	0.40
2350	Sheared	0.7	0.42
2420	Sheared	1.4	0.37

THE MODEL RISER AND THE AVAILABLE DATA

The NDP model riser experiment was carried out by the Norwegian Marine Technology Research Institute (Marintek) in 2003, by horizontally towing a flexible cylinder in a water tank. The cylinder is of 38 m length with a length-to-diameter (L/D) ratio of 1,400. The model riser was tested for uniform as well as linearly sheared current profiles. Riser response was measured using 24 strain sensors (one sensor failed for some test runs; hence, in some cases, only 23 strain sensors were available) and 8 accelerometers for the CF direction; similarly, in the IL direction, measurements from 40 strain sensors and 8 accelerometers were available. Additional details on the NDP experiments that relate to the test setup and other physical properties of the model riser may be found in the work of Braaten and Lie [4] and Trim et al. [2].

Among the six data sets available at the VIV data repository [5], four of them were obtained from tests on bare risers. Table 1 summarizes current characteristics and RMS (root-mean-square) CF displacement values normalized with respect to the diameter, D, of the cylinder. Because of the large RMS displacement values that were computed from data in these four tests, the riser response is thought to be associated with VIV and, as such, these four tests are well suited for this study. Note that, in Table 1, the RMS CF displacement reported is based on the entire length of record and the largest value from all the eight accelerometer loggers was considered.

CHARACTERISTICS OF THE RISER VIV RESPONSE

In the tests considered, the NDP model riser exhibits complex response characteristics including non-stationary behavior, higher harmonics, and the presence of traveling waves. These characteristics associated with VIV of the riser are next analyzed and discussed using mathematical techniques such as Hilbert and wavelet transforms.

Non-Stationary Characteristics: Variation of Displacement Amplitude and Phase of Orbits

Although higher harmonics are commonly observed in the strain and acceleration response of a riser experiencing VIV, their contribution to the displacement response is somewhat diminished. Let us assume that the IL displacement, $x(t)$, and the CF displacement, $y(t)$, may be expressed as single-frequency trigonometric functions, such that

$$x(t) = A_x(t) sin[\omega_x(t) \cdot t + \theta(t)]; \;\; y(t) = A_y(t) sin[\omega_y(t) \cdot t] \quad (1)$$

where $A_x(t)$ and $A_y(t)$ are the instantaneous IL and CF displacement amplitudes, respectively; similarly, $\omega_x(t)$ and $\omega_y(t)$ are the instantaneous IL and CF displacement angular frequencies, respectively. The phase angle, $\theta(t)$, which separates the IL displacement from the CF displacement, is of particular interest here because different values of $\theta(t)$ are associated with different shapes of the riser displacement orbits [6]. For clarity, a schematic diagram showing displacement orbits for various values of $\theta(t)$ is presented in Fig. 1 where the horizontal axis represents IL displacement and the vertical axis represents CF displacement. The direction of oscillation is indicated using three dots, i.e., the motion starts at the largest dot, then proceeds to the smaller ones. Furthermore, four distinct orbit types are plotted using four different colors. When $\theta = \pi$, the displacement orbit assumes a figure-eight shape and the riser IL motion is from left to right when passing the outermost CF positions. In accordance with terminology used by Modarres-Sadeghi et al. [7], this orbit shape is characterized as counter-clockwise figure-eight and is colored red. Similarly, the orbit shape associated with $\theta = 0$ is characterized as clockwise figure-eight and is colored blue. When $\theta = -\pi/2$, the displacement orbit takes the shape of the letter C and is colored green; finally, when $\theta = \pi/2$, the displacement orbit takes the shape of a mirrored letter C and is colored cyan. When $\theta(t)$ takes on intermediate values different from ones explicitly noted above, e.g., when $\theta = -\pi/4$, the associated displacement orbit takes the shape of a hybrid of a clockwise figure-eight and a letter C.

Given the measured IL and CF displacement time series, $x(t)$ and $y(t)$, their instantaneous amplitudes, $A_x(t)$ and $A_y(t)$, as well as the phase angle, $\theta(t)$, may be estimated from their analytic signals constructed using the Hilbert transform. Details related to the form and construction of the analytic signal and background related to the Hilbert transform may be found in the literature (see, for example, Bendat and Piersol [8]).

Using a uniform current data set, NDP2120, as an example, the displacement orbits measured at accelerometer no. 5 ($x/L = 0.56$) are compared, over a short interval of time, with ones reconstructed from estimates of $A_x(t)$, $A_y(t)$ and $\theta(t)$. In Fig. 2, the orbits are plotted using the same color designations that were used in Fig. 1. Orbit shapes constructed from theoretical considerations (i.e., on the basis of Eq. 1) using estimated phases and amplitudes are close to the measured orbits as seen in Fig. 2 where the estimated phase angles are noted for each plot. That the reconstructed displacement orbits (dashed lines) match the measured orbits reasonably well is an indication that the instantaneous displacement amplitudes $A_x(t)$, $A_y(t)$, and the phase angles, $\theta(t)$, may be quite accurately estimated with the help of the Hilbert transform.

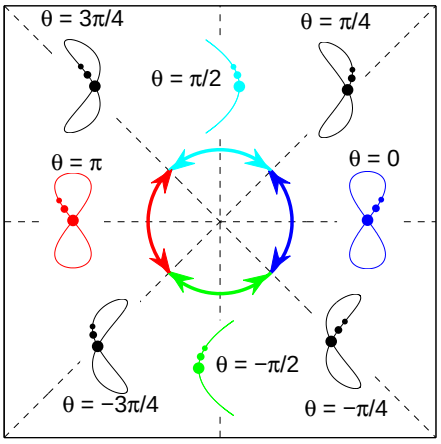

Figure 1. Displacement orbits associated with different values of θ as defined in Eq. 1.

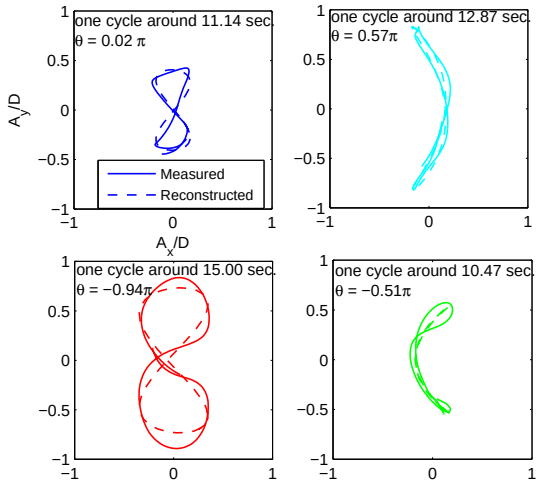

Figure 2. Displacement orbits: measured versus reconstructed using estimation of instantaneous amplitudes ($A_x(t)$ and $A_y(t)$) and phase angle, $\theta(t)$.

The time-varying phase angles, $\theta(t)$, and the CF displacement amplitudes, $A_y(t)$, are estimated for each time instant at the eight locations where the displacement (acceleration) measurements are available. Results for the uniform current data set, NDP2120, are plotted in Fig. 3 while results for the sheared current data set, NDP2350, are plotted in Fig. 4. In these figures, the different colors indicate associated phase angles (consistent with the color coding used in Fig. 1); for example, the blue color indicates that the phase angle lies in the range, $-\pi/4 < \theta < \pi/4$.

Observations with the uniform current data set, NDP2120, suggest that (i) the phase angles as well as the CF displacement amplitudes vary considerably with time and spatial location (which is an indicator of obvious non-stationary character in the

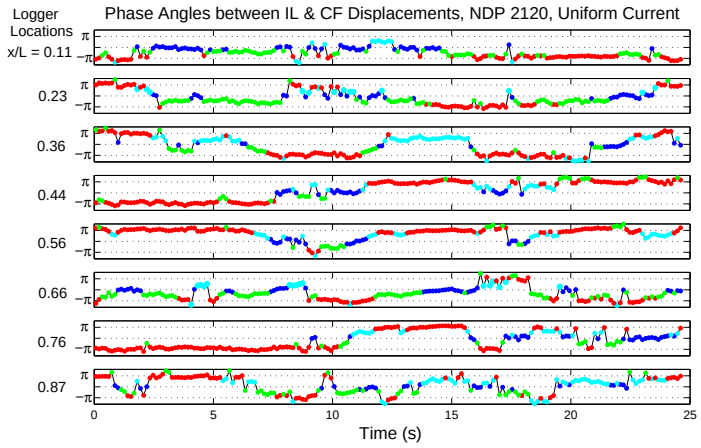

(a)

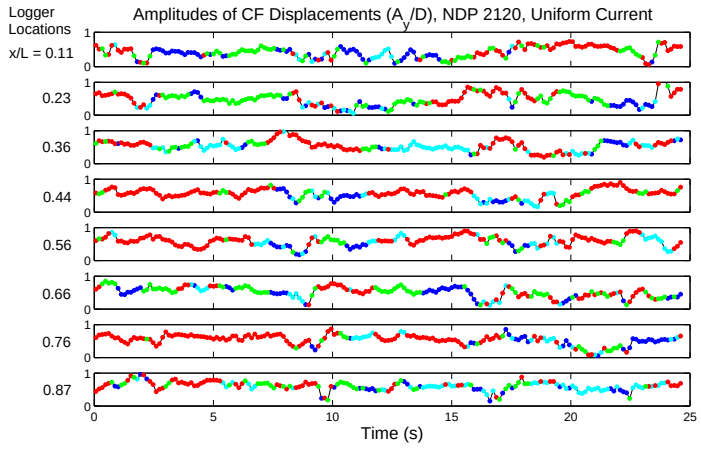

(b)

Figure 3. The uniform current data set, NDP2120: (a) Phase difference between IL and CF displacements; and (b) Amplitude of CF displacement.

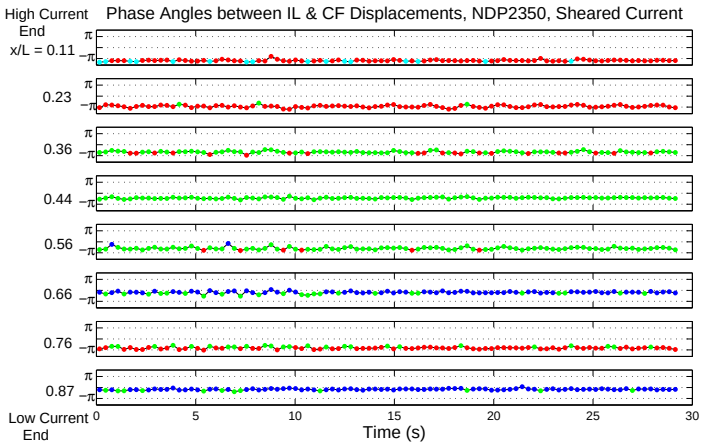

(a)

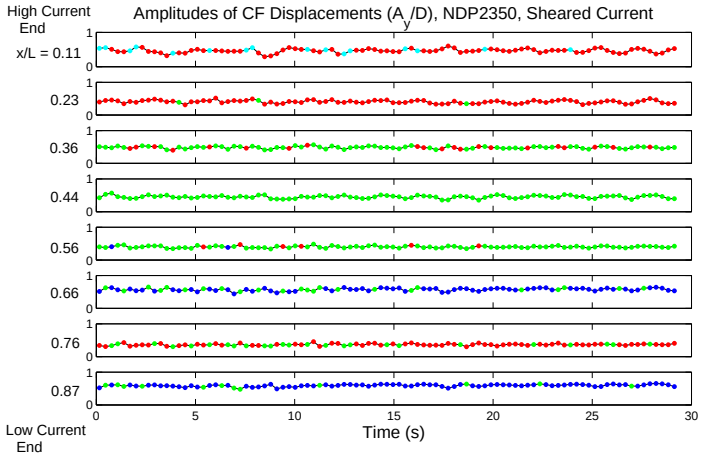

(b)

Figure 4. The sheared current data set, NDP2350: (a) Phase difference between IL and CF displacements; and (b) Amplitude of CF displacement.

VIV response); (ii) the largest CF amplitude is slightly in excess of $1 \times D$ (where D is the riser diameter)and it occurs at the second sensor ($x/L = 0.23$) and around 24 seconds into the record. In contrast, for the sheared current data set, NDP2350, the estimated phase angles and the CF displacement amplitudes take different values at the eight different accelerometer locations, but they remain almost unchanged with respect to time. In summary, the riser motions resulting from uniform current profiles exhibit much stronger non-stationary characteristics than those excited by sheared currents.

Higher Harmonics and Varying Frequency Content

The strong non-stationary characteristics of the riser response observed for the NDP2120 data set suggests that the use of the Fourier transform alone on an entire record may not give an adequate representation of the time-varying frequency content of the riser response. Instead, using a continuous wavelet transform (CWT), variation with time in the dominant frequencies of the signal both in the first and in higher harmonics, when present, can be easily understood by studying CWT scalograms (which indicate the squared modulus of the wavelet transform as it varies with time and scale). Additional details related to the wavelet transform and its applications on civil engineering may be found in the literature (see, for example, Kijewski and Kareem [9]).

Scalograms, using the Morlet wavelet function, of strain measurements at the location, $x/L = 0.11$, for the uniform current and the sheared current data sets, NDP2120 and NDP2350, respectively, are presented in Fig. 5. The warm colors indicate the time intervals and frequency bands where the energy is concentrated. The scalogram for the NDP2120 data set (uniform current case) shows presence of a dominant first mode (around 7 Hz) as well as a third harmonic (around 21 Hz) in the measured strains. Interestingly, the first mode does not persist to the same degree over the entire duration; also, the frequencies associated with both first and third harmonics show some variation with time. These observations, again, confirm the non-stationary character of the riser response of NDP2120. In contrast, though the scalogram for the NDP2350 data set (sheared current case) also shows energy distribution at the first mode (around 3 Hz) and at the third harmonic (around 10 Hz) in the measured strain signal, the first mode does persist for the entire duration and its

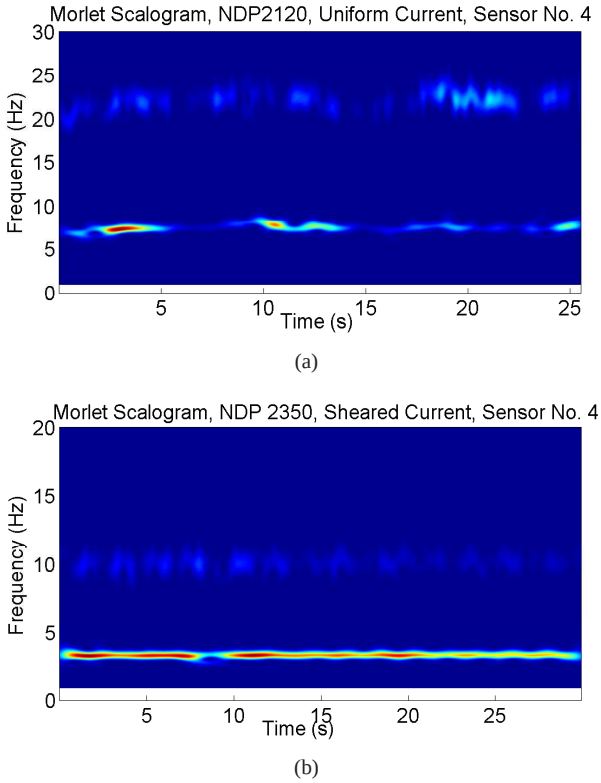

Figure 5. Morlet scalograms of strains measured at location, $x/L = 0.11$, for (a) the uniform current data set, NDP2120; and (b) the sheared current data set, NDP2350.

frequency remains almost constant while the third harmonic, too, only shows very slight variation with time. It is the persistence and steadiness of the dominant first mode that leads to relatively more stationary characteristics for the NDP2350 case (sheared current) compared to the NDP2120 case (uniform current), as was noted earlier while studying the amplitudes and phases of riser displacements in Figs. 3 and 4.

Traveling Waves

In addition to clear indication of non-stationary characteristics and the presence of higher harmonics in the NDP model riser's VIV response, traveling wave features are also evident in the response of the riser excited either by uniform or sheared currents. Waterfall plots of the CF bending strains measured at the 24 locations are presented in Fig. 6, where the abscissa indicates time and the ordinate indicates location along the riser.

For the two uniform current data sets, we find that traveling wave characteristics persist in the response for about 50% of the length of the record (representing more than fifty CF motion cycles for each data set). This traveling wave pattern is weak and occurs only over a portion of riser, not its entire length. Moreover, for some intervals of the record, energy is generated near the "upper" end (closer to $x/L = 0$) and propagates downward while, over other intervals, energy is generated near the "lower" end (closer to $x/L = 1$) and propagates upward. This latter finding may likely be because with a uniform current profile, there is equal propensity for any portion of the riser to be the power-in region; the wave propagation direction may then be determined by competition between these candidate lock-in regions. Figure 6(a) shows a one-second segment of the CF bending strains from the NDP2120 uniform current data set; it is clear that a wave is generated at a location around $x/L = 0.7$ and this wave travels upward. Similar studies on the two available sheared current data sets indicate that a traveling wave pattern persists for almost the entire length of record; also, this traveling wave pattern is much clearer and evident over the entire length of the riser. Energy in the motion is always transferred to the riser from the higher current end (which we referred to as the "upper" end when discussing the uniform current data), and propagates downward in a traveling wave towards the lower current end (the "lower" end). In Fig. 6(b), the repeated diagonal stripes are clear evidence of a strong traveling wave that is dominant over almost the entire length of the riser; it is only in a small region near the upper end ($x/L = 0$) that the riser response is well represented by a standing wave, which presumably arises due to reflections of traveling waves.

WEIGHTED WAVEFORM ANALYSIS

Weighted Waveform Analysis (WWA) is a computational procedure that is widely used to analyze and reconstruct the response over the entire length of a riser from measurements at a limited number of sensors (for details, see the studies by Trim et al. [2] and Lie and Kaasen [3]).

Assume that the riser displacement, x, at location, z, and at time, t, may be expressed as a weighted sum of N assumed modes. Thus, we have:

$$x(z,t) = \sum_{i=1}^{N} w_i(t)\varphi_i(z) \tag{2}$$

where it is assumed that by using N (not necessarily consecutive) modes, one can approximately represent the riser displacement at any location, z. Also, $\varphi_i(z)$ represents the $n_i{}^{\text{th}}$ mode shape of the displacement, while $w_i(t)$ represents the time-varying modal weight to be applied to the $n_i{}^{\text{th}}$ mode shape.

If the assumed modes are sinusoidal in shape, i.e., if $\varphi_i(z) = \sin(n_i\pi z/L)$ where L is the riser length, then the bending strain, which equals the product of the riser radius, R, and the local curvature, x'', may be expressed as follows:

$$\varepsilon(z,t) = Rx''(z,t) = \sum_{i=1}^{N} Rw_i(t)\varphi_i''(z) \tag{3}$$

where $\varphi_i''(z) = -(n_i\pi/L)^2\,\varphi_i(z)$ is the curvature of the $n_i{}^{\text{th}}$ mode shape.

Given strain measurements or, equivalently, curvature measurements at M logger locations, z_j (where $j = 1$ to M), WWA requires solution of a system of equations in matrix form:

$$\mathbf{Aw} = \mathbf{b} \tag{4}$$

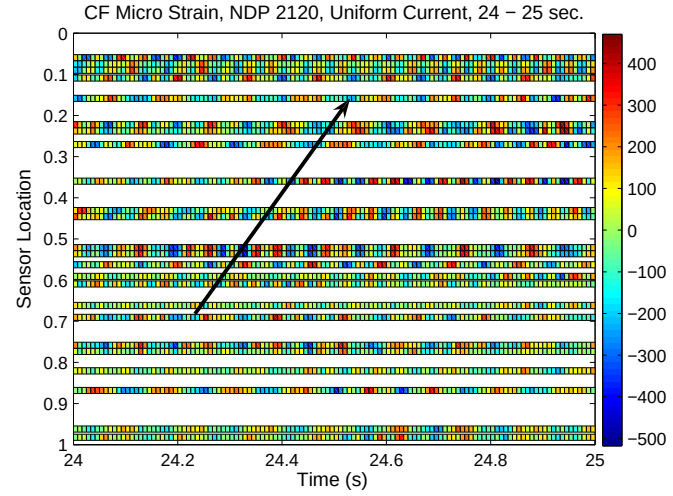

(a)

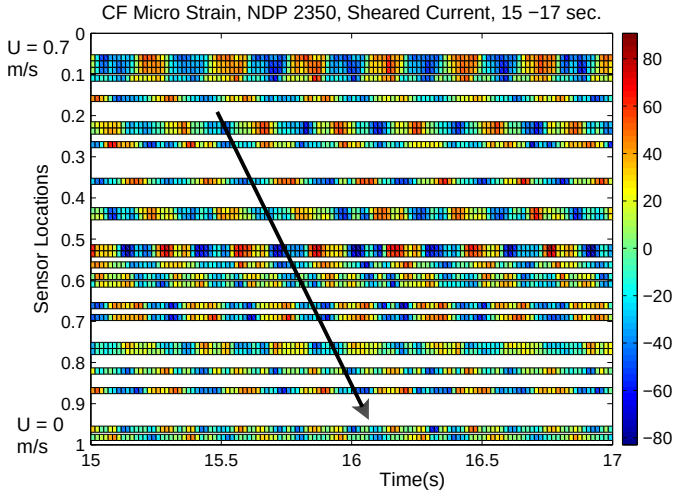

(b)

Figure 6. Traveling wave patterns for (a) the uniform current data set, NDP2120; and (b) the sheared current data set, NDP2350.

where the matrix, **A**, comprises curvatures of the assumed mode shapes at all the logger locations and the vector, **b**, is formed from the measured strains at all loggers. In expanded form, we have:

$$\mathbf{A} = \begin{bmatrix} \varphi''^{1}_{1} & \varphi''^{1}_{2} & \cdots & \varphi''^{1}_{N} \\ \varphi''^{2}_{1} & \varphi''^{2}_{2} & \cdots & \varphi''^{2}_{N} \\ \vdots & \vdots & \vdots & \vdots \\ \varphi''^{M}_{1} & \varphi''^{M}_{2} & \cdots & \varphi''^{M}_{N} \end{bmatrix}; \mathbf{w} = \begin{bmatrix} w_1 \\ w_2 \\ \vdots \\ w_N \end{bmatrix}; \mathbf{b} = \begin{bmatrix} \varepsilon_1/R \\ \varepsilon_2/R \\ \vdots \\ \varepsilon_M/R \end{bmatrix} \quad (5)$$

where $\varphi''^{j}_{i} = -(n_i\pi/L)^2 \sin(n_i\pi z_j/L)$ is the curvature of the n_i^{th} mode shape at logger location, z_j, and $\varepsilon_j = \varepsilon(z_j,t)$. Equation 4 is a linear system of M equations with N weights to be estimated. At any instant of time, t, as long as $N \leq M$, the modal weights vector, **w**, may be solved for in a least squares sense. Thus, we have:

$$\mathbf{w}(t) = \left(\mathbf{A}^T\mathbf{A}\right)^{-1}\mathbf{A}^T\mathbf{b}(t) \quad (6)$$

Finally, the riser response, such as the CF bending strain, at any location, z, may be reconstructed using Eq. 3. The fatigue damage rate at that location may then be estimated from the entire reconstructed strain time series. The WWA method, as presented above, seems simple and straightforward to apply. However, two points need to be noted. First, the number of available sensors, M, limits the number of modes, N, that may be included in the WWA scheme, i.e., $N \leq M$; this indicates that a larger number of available sensors allows a greater number of modes to be included, which will generally lead to more accurate reconstruction of the riser response. Second, given a specified arrangement of available sensors, the set of assumed modes need to be selected a priori for the WWA scheme; these selected mode shapes directly control the quality of reconstruction of the riser response.

FATIGUE DAMAGE ESTIMATION

The NDP model riser was densely instrumented; the CF response was recorded using twenty-four strain sensors and eight accelerometers. If all of the thirty-two sensors are used with the WWA procedure, reconstruction of the riser response and estimation of the fatigue damage rate over the length of the riser would likely be more accurate. However, in the field, real deepwater drilling risers are almost never instrumented as densely as the NDP model riser, due to the high cost of the deployment, maintenance, and data retrieval from all the loggers. The WWA procedure is useful for the analysis of real drilling risers as long as its response reconstructions are accurate even with a small number of sensors. In this study, we consider riser response reconstruction using WWA with only eight strain sensors. Fatigue damage rates are then estimated from the reconstructed strains at the locations of all of the twenty-four instrumented sensors. By iterating over numerous different combinations of the selected eight strain sensors as inputs (from among all of the twenty-four available sensors on the riser), we seek to identify the optimal locations for eight sensors on the riser by cross-validation whereby WWA-based predicted strains and fatigue damage rates at all the twenty-four locations are compared with strains and fatigue damage rates based on the actual recorded measurements there.

Thirty-four combinations involving eight different loggers are considered in this study. Figure 7 shows the locations of the eight sensors for these thirty-four combinations. For example, the first group (labeled G1) contains sixteen combinations, each of which includes eight spatially contiguous sensors (from the available twenty-four); similarly, the second group (G2) contains six combinations where six sensors are near the top (higher current) end and two additional sensors are located at the middle, at a location one-fourth of the riser's length from the bottom (low current) end, or at the bottom end. Other groups representing different sensor arrangements are also indicated in Fig. 7. For illustration, the sheared current data set, NDP2350, with Combination No. 33 (see Fig. 7) is chosen to discuss estimation of

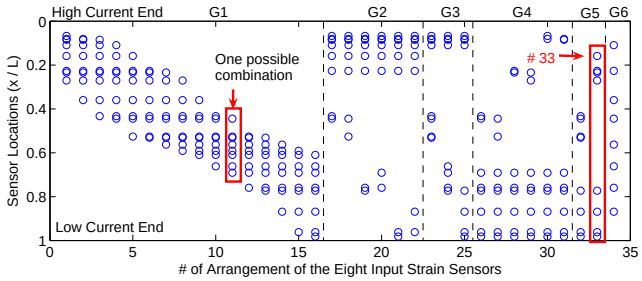

Figure 7. Thirty-four combinations of eight input strain sensors used with the WWA procedure to predict fatigue damage.

the fatigue damage rate using the WWA method and the measurements from the eight strain sensors. The reason for choosing Combination No. 33 is because it proved to be one of the best combinations for accurate fatigue predictions with all the four NDP data sets.

Reconstruction of the response over the riser's entire length using the WWA method from only eight sensors raises questions related to selection of the assumed modes. In this study, we propose an energy-based mode selection procedure according to which only the dominant frequencies (and associated modes) are selected and fitted within the WWA scheme. The results suggest that the proposed mode selection method preserves the influence of the first as well as higher harmonics in the reconstructed riser response. Some details related to the mode selection method are presented next.

Given the CF strain time series, $\varepsilon_j(t)$, measured at location, z_j (where $j = 1,\ldots,8$), its power spectral density (PSD), $PSD_j(f)$, describes the energy distribution by frequency of the riser response at that location. As illustrated in Fig. 8(a), the eight input strain power spectra indicate very similar frequency content; all these spectra show the presence of the first, third, and fifth harmonics in the response. The summation of the PSDs for all the eight sensors, i.e., $\sum_j PSD_j(f)$ (see Fig. 8(b)) is assumed to account for the energy distribution by frequency of the entire riser and is, therefore, used for the WWA mode selection. First, the two highest peaks in Fig. 8(b), which represent the first and third harmonics, are selected as major modes. The associated mode numbers are determined by comparing the peak frequencies with the estimated natural frequencies of the riser. For the sheared current data set, NDP2350, assuming an added mass coefficient, $C_a = 1$, the two major modes are identified as the fifth and the fourteenth modes, respectively. Second, each Fourier frequency is associated with estimated natural frequencies of the riser; thus, another two modes—the fourth and the twenty-third—that have the largest (summed) PSD values, but which are different from the two major modes, are selected as minor modes. The two major modes as well as the two minor modes are indicated on the (summed) PSD plot in Fig. 8(b). The results show that the selected four modes cover the first, third, and fifth harmonics of the input signals, and assure accurate response reconstruction over the entire riser span as is discussed next.

After selection of the assumed modes for the WWA procedure, the response over the entire length of the riser may be

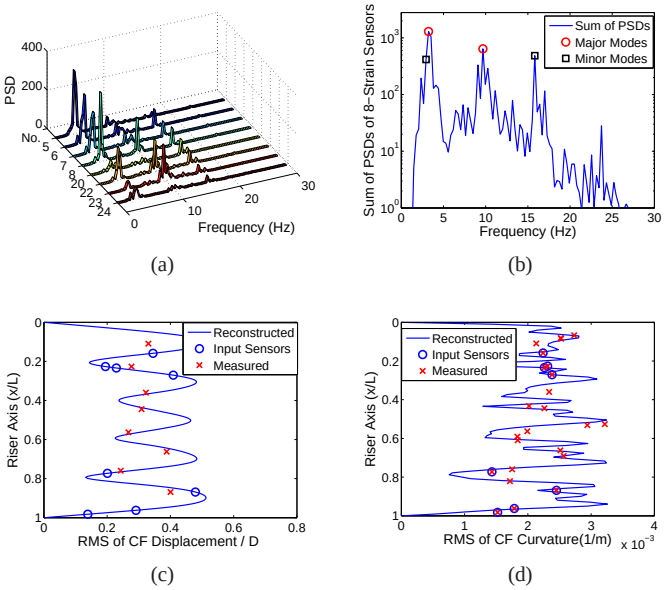

Figure 8. The WWA procedure applied with the eight strain sensors of Combination No. 33 for the NDP2350 (sheared current) data set: (a) PSDs of the strains measured at the eight sensors; (b) Summation of the PSDs and identification of the selected modes; (c) RMS displacements, reconstructed vs. measured; and (d) RMS curvatures, reconstructed vs. measured. (PSD units: $(\mu\varepsilon)^2$/Hz.)

reconstructed after obtaining the time-varying modal weights. Normalized CF RMS displacements reconstructed (blue line) and measured values obtained from the eight accelerometers (red crosses) are plotted in Fig. 8(c). Similarly, RMS values of the CF curvature reconstructed (blue line) and measured values obtained from the twenty-four strain sensors (red crosses) are plotted in Fig. 8(d). In Figs. 8(c) and (d), the eight blue circles indicate the locations of the eight input sensors that are included in Combination No. 33. The results suggest that the reconstructed riser displacements are dominated by the fifth mode and, in general, they match the measured displacement values reasonably well. Also, the reconstructed curvatures are dominated by the fifth and fourteenth modes (the first and third harmonics); in general, these also match curvature values inferred from measurements at the twenty-four strain sensors.

Following application of the WWA procedure, fatigue damage rates are computed for various locations along the riser using the rainflow cycle-counting algorithm and Miner's rule. An F-2 S-N curve is assumed as follows:

$$N = aS^{-b} \tag{7}$$

where N is the number of cycles to failure at the stress range S; also, $a = 4.266 \times 10^{11}$ and $b = 3.0$ are parameters of the F-2 S-N curve [10].

The fatigue damage rates resulting from the WWA-based reconstructed strains are compared with those based directly on measurements at the twenty-four locations where strain loggers were present. A parameter, the Damage Ratio (DR), representing the ratio of the estimated fatigue to the measured fatigue, is used

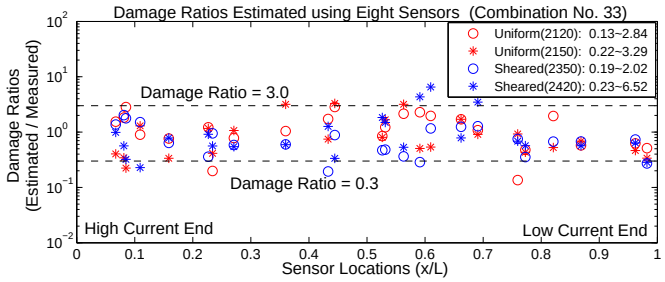

Figure 9. Damage ratios estimated at various locations using the WWA procedure with the eight sensors of Combination No. 33.

as an indicator of the "quality" of the reconstruction. This Damage Ratio, calculated at the location of the strain sensor under consideration (say, sensor no. j), is then expressed as follows:

$$DR = \frac{n_e S_e^b}{n_m S_m^b} \tag{8}$$

where n_e and S_e represent, respectively, the number of cycles and the equivalent stress (strain) range based on the reconstructed strain time series at sensor no. j; n_m and S_m are the corresponding quantities obtained from the strain time series directly measured at sensor no. j.

Damage ratios, estimated at the twenty-four locations from the eight sensors of Combination No. 33, are plotted in Fig. 9. The results show that, for the four data sets which include two uniform current data sets and two sheared current data sets, most of the damage ratios fall in the range from 0.3 to 3.0; the lowest and highest damage ratios are 0.13 and 6.52, respectively. This suggests that, in the worst case, the WWA-based fatigue damage rate can be up to seven times smaller or larger than the correct value.

Damage rates estimated from eight sensors for all the 34 considered combinations (defined in Fig.7) are illustrated by box-whisker plots in Fig. 10. Results for the two uniform current data sets and results for the two sheared current data sets are presented in Fig. 10(a) and Fig. 10(b), respectively. Each vertical bar represents one of the 34 combinations; the height of the bar describes the range of the twenty-four damage ratios for the selected combination of eight sensors; in addition to the extremes (minimum and maximum), the 25^{th} and 75^{th} percentile damage ratios are also indicated. The shorter a bar is, the more precise is the estimation for that combination of eight sensors; the closer a bar is to 1.0, the more accurate is the estimation for that combination. Good combinations of eight sensors for the NDP model riser that ensure precise and accurate estimation of fatigue damage rate for all the four data sets are indicated by green arrows in Figs. 10(a) and (b). It is seen that eight sensors instrumented over a large portion of the riser, e.g., four sensors near one end and four sensors near the other end (as in Combination Nos. 25 or 33), generally provide better fatigue damage estimation than eight clustered sensors (as in Combinations Nos. 1 to 16). Note that the various combinations and location of the eight sensors in each case are given in Fig.7.

IMPROVED FATIGUE DAMAGE ESTIMATION: NON-STATIONARY RESPONSE CHARACTER AND TRAVELING WAVES

We have discussed above that non-stationary characteristics and traveling waves are often evident in the VIV response of a riser. The WWA scheme with a small number of sinusoidal basis functions serving as modes can, only to a limited extent, capture the influence of traveling waves. Moreover, the modes selected with the WWA scheme are based on the strain power spectra estimated from the entire record, and neglect possible frequency variation in energy content in these spectra as a function of time (i.e., during the record). We present here an illustrative example wherein we attempt to better capture any non-stationary response characteristics and the effect of traveling waves, in more accurate fatigue damage estimation. The uniform current data set, NDP2120, is employed in this example since it shows evidence of strong non-stationary characteristics and a moderate traveling wave pattern in the riser response. The strains were measured at twenty-four sensors along the riser's length. From among these sensors, we first select one as the "target" sensor and use the remaining twenty-three sensors as "input" sensors; we use the empirical WWA method along with measurements from the input sensors to reconstruct the strain time series at the location of the target sensor. We estimate the fatigue damage rate at the location of the target sensor from the estimated (reconstructed) strain there and compare it with that based on the actual measurements at the target sensor using a Damage Ratio as before.

In order to account for non-stationary response characteristics in improved estimates of the Damage Ratio, we first divide the entire duration of the record into N_s shorter segments. We reconstruct the target strain for each data segment by using the associated segment of all the input strains, and then estimate that segment's fatigue damage. By iterating over all the data segments, the fatigue damage for the entire record is computed as the sum of the fatigue damage estimates from all the shorter segments. This Damage Ratio (for any target sensor location), obtained by combining all the shorter segments of data, is defined as follows:

$$DR = \frac{\sum_{s=1}^{N_s} n_{e,s} S_{e,s}^b}{n_m S_m^b} \tag{9}$$

where s refers to the segment number of the record that is assumed to consist of N_s segments. The denominator in Eqs. 8 and 9 is the same, while the numerator in Eq. 9 refers to the summation of the fatigue damage caused by all the estimated N_s strain segments at the target sensor location.

We employ the WWA method with Eq. 9 to refine fatigue damage estimates that account for non-stationary response. In order to also better account for the influence of traveling waves evident in the riser response, an enhancement to the WWA method which is termed as the "modified WWA" method is also employed. The modified WWA method introduces cosine basis functions to complement the sine functions for each frequency component in the WWA method. Additional details on the "modified WWA" method can be found elsewhere [11].

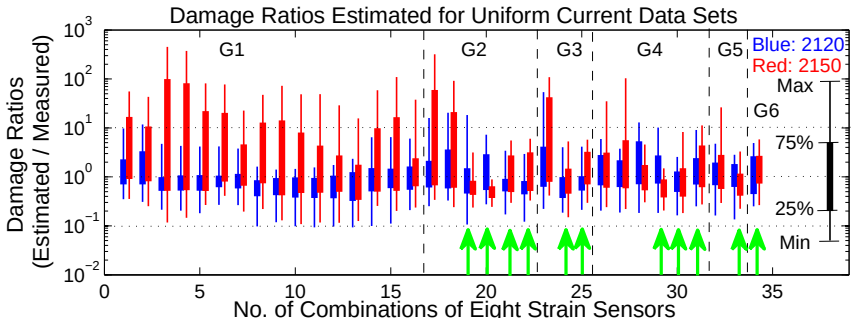

(a)

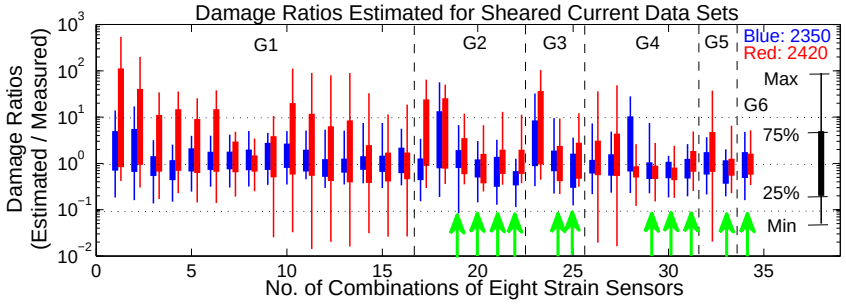

(b)

Figure 10. Damage ratios estimated from eight sensors considering of all the 34 combinations for (a) the two uniform current data sets; (b) the two sheared current data sets.

In the following, for the uniform current data set, NDP2120, we employ strain sensor no. 4, which shows some non-stationary response characteristics (see Fig. 5(a)), as the target sensor to illustrate refinements to the fatigue damage estimation procedure. As shown in Fig. 5(a), the 26 sec. long record may be divided into four segments—i.e., 0 to 5sec., 5 to 10 sec., 10 to 15 sec., and 15 to 26 sec. Each of these segments is then treated as stationary separately rather than using the entire record as stationary. Damage ratios estimated under two different assumptions—stationary (i.e., based on the entire record) or non-stationary (based on the shorter segments)—and using two different empirical (i.e., the WWA and the modified WWA methods) are presented in Table 2. Note that with both of the empirical methods, six modes are employed in the target sensor strain reconstruction. Note, too, that the actual modes employed change slightly in the four different segments. As can be seen in Table 2, for target sensor no. 4 with the NDP2120 data set, by consideration of non-stationary characteristics of the response, the accuracy of the estimated damage ratios is improved by about 6%—i.e., from 0.34 to 0.40, with the WWA method and from 0.56 to 0.62 with the modified WWA method. More systematic consideration of the effect of traveling waves possible by use of the modified WWA method improves the accuracy in fatigue damage prediction by about 22%—i.e., from 0.34 to 0.56 if the entire record is used (stationary assumption), or from 0.40 to 0.62 if the response is treated as non-stationary and the record is processed in segments.

Table 2. Damage Ratios estimated at the location of Strain Sensor No. 4 ($x/L = 0.11$) for the NDP2120 (uniform current) data set.

WWA		Modified WWA	
Stationary	Non-stationary	Stationary	Non-stationary
0.34	0.40	0.56	0.62

CONCLUSIONS

This study showed that mathematical tools, such as the use of the Hilbert transform and the wavelet transform, are useful to study complex characteristics of the vortex-induced vibration response of a riser. Using the Hilbert transform, instantaneous amplitudes and phase angles (associated with displacement orbits) can be estimated from measured cross-flow and in-line displacements; these can then be used to examine non-stationary characteristics of the riser response. Scalograms (describing squared coefficients of the wavelet transforms) of the measured strain signals help to reveal the presence and variation of different harmonics in the riser response. In addition to noting the non-stationary characteristics and the presence of higher harmonics in the NDP model riser response, traveling wave patterns were also observed in the VIV response, albeit with different characteristics for uniform versus sheared currents.

The Weighted Waveform Analysis (WWA) method was employed to reconstruct the riser response at various locations along the NDP model riser by making use of eight strain sensors. By using the proposed mode selection approach in WWA, the first as well as higher harmonics could be preserved in the reconstructed riser response. Fatigue damage rates estimated based on the reconstructed strains were compared with those based directly on the recorded strain measurements. It was shown that, if properly placed, as few as eight sensors could provide reasonably accurate estimates of the fatigue damage rate over the entire riser length. Finally, accounting for non-stationary characteristics and for ev-

idence of traveling waves in the response in empirical methods was shown, with an illustrative example, to lead to improved fatigue damage estimation.

ACKNOWLEDGMENT

Financial support and technical guidance provided to the first two authors by BP America Production Co. is greatly appreciated.

REFERENCES

[1] Chasparis, F., Modarres-Sadeghi, Y., Hover, F., Triantafyllou, M., Tognarelli, M., and Beynet, P., 2009. "Lock-in, transient and chaotic response in riser VIV". In 28th International Conference on Ocean, Offshore and Arctic Engineering, OMAE 2009.

[2] Trim, A., Braaten, H., Lie, H., and Tognarelli, M., 2005. "Experimental investigation of vortex-induced vibration of long marine risers". *Journal of Fluids and Structures*, **21**, pp. 335–361.

[3] Lie, H., and Kaasen, K., 2006. "Modal analysis of measurements from a large-scale VIV model test of a riser in linearly sheared flow". *Journal of Fluids and Structures*, **22**, pp. 557–575.

[4] Braaten, H., and Lie, H., 2004. NDP riser high mode VIV tests. Main Rerport No. 512394.00.01. Tech. rep., Norwegian Marine Technology Research Institue.

[5] Center for Ocean Engineering, MIT, 2007. Vortex induced vibration data repository. http://oe.mit.edu/VIV.

[6] Jauvtis, N., and Williamson, C., 2004. "The effect of two degrees of freedom on vortex-induced vibration at low mass and damping". *Journal of Fluid Mechanics*, **509**, pp. 23–62.

[7] Modarres-Sadeghi, Y., Mukundan, H., Dahl, J., Hover, F., and Triantafyllou, M., 2010. "The effect of higher harmonic forces on fatigue life of marine risers". *Journal of Sound and Vibration*, **329**, pp. 43–55.

[8] Bendat, J., and Piersol, A., 2000. *Random Data Analysis and Measurement Procedures, Third Edition*. A Wiley-Interscience Publication, New York.

[9] Kijewski, T., and Kareem, A., 2003. "Wavelet transforms for system identification in civil engineering". *Computer-Aided Civil and Infrastructure Engineering*, **18**, pp. 339–355.

[10] Bai, Y., Bhattacharyya, R., and McCormick, M., 2001. *Pipelines and Risers*. Elsevier Science Ltd.

[11] Shi, C., Manuel, L., and Tognarelli, M., 2010. "Alternative empirical procedures for fatigue damage rate estiamtation of instrumented risers undergoing vortex-induced vibration". In 29th International Conference on Ocean, Offshore and Arctic Engineering, OMAE 2010.